

Two Heads are Better than One: Geometric-Latent Attention for Point Cloud Classification and Segmentation

Hanz Cuevas-Velasquez¹

hanz.c.v@ed.ac.uk

Antonio Javier Gallego²

ajgallego@dlsi.ua.es

Robert B. Fisher¹

rbf@inf.ed.ac.uk

¹ School of Informatics
University of Edinburgh
Edinburgh, UK

² Department of Software and Computing
Systems
University of Alicante,
Alicante, Spain

Abstract

We present an innovative two-headed attention layer that combines geometric and latent features to segment a 3D scene into semantically meaningful subsets. Each head combines local and global information, using either the geometric or latent features, of a neighborhood of points and uses this information to learn better local relationships. This Geometric-Latent attention layer (Ge-Latto) is combined with a sub-sampling strategy to capture global features. Our method is invariant to permutation thanks to the use of shared-MLP layers, and it can also be used with point clouds with varying densities because the local attention layer does not depend on the neighbor order. Our proposal is simple yet robust, which allows it to achieve competitive results in the ShapeNetPart and ModelNet40 datasets, and the state-of-the-art when segmenting the complex dataset S3DIS, with 69.2% IoU on Area 5, and 89.7% overall accuracy using K-fold cross-validation on the 6 areas.

1 Introduction

Robotics, autonomous driving, and related areas rely heavily on information captured by 3D sensors like RGB-D cameras, stereo cameras, and LiDARs. This information provides to the agent (robots or cars) the 3D location of their surroundings, which can be processed and used in tasks like scene understanding, path planning, navigation, among others [4, 5, 25]. One of the most used approaches to detect objects in 3D space is point cloud segmentation. A point cloud is a set of points in 3D, usually unordered and sparse; some regions can be densely populated and others empty. This type of non-grid structured data is difficult to be used with convolution operators with the same efficiency as their 2D counterpart.

Various approaches have been proposed to handle such data. Some approaches project the 3D raw data into a regular structure (e.g. voxels) where 3D convolutions can be used [10, 17, 22, 23, 31, 39]. Other approaches use multilayer perceptrons (MLP) to process

point clouds directly [19, 20, 29]. A third approach is to project the points to an intermediate grid structure where 2D convolutions can be used [9, 15, 35]. Lately, with the success of transformers and attention mechanisms in the area of natural language processing (NLP) [30], these methods are starting to be used for 3D point cloud problems [6, 21].

This paper proposes a multi-head attention layer called Geometric-Latent Attention (Ge-Latto) to segment and label subsets of the point cloud. Ge-Latto is a two-headed local attention layer that evaluates a patch inside the point cloud and tries to find good relationships between the neighbor points. Unlike other works that combine all the features indiscriminately [13, 38], each attention head focuses on a specific type of feature. One head is in charge of finding good geometric relations and the other in finding relationships among the latent features of the network. Similar to [15], we use an encoder-decoder network with residual connections. Each layer of the encoder sub-samples the input points, groups the points into neighborhoods, and uses our Ge-Latto layer to find local-spatial relationships from the latent and geometric features of neighbor points. The neighbors are found using radius neighborhoods instead of k-nearest-neighbors (kNN). The network increases this radius in each layer to increase the field of view and find relationships in bigger neighborhoods. In the decoder part, we up-sample the points using tri-linear interpolation. To ensure that in each sampled layer the network learns useful features, we add auxiliary losses similar to PSPNet [37] and RetinaNet [14]. In other words, the network predicts the segmentation for each sample size as seen in Figure 1. Our approach is also invariant to permutation because all the layers are shared MLPs.

The main contributions of this paper are: **a)** A novel two-headed attention layer that is able to combine efficiently the geometric and latent information of unordered point clouds with variable densities for semantic segmentation and shape classification. **b)** A pyramid-based encoder-decoder architecture with multi-resolution outputs and auxiliary losses to leverage feature patterns at different resolutions. **c)** State of the art performance on the complex dataset S3DIS. Not only in the area 5, but also in the k-fold cross-validation overall accuracy, as well as competitive results in the ShapeNetPart and ModelNet40 datasets.

2 Related Work

Recent works focus on how to handle unordered 3D points and find spatial relationships between them to better segment a point cloud. This section briefly reviews these methods and groups them into 4 categories.

Volumetric-based methods. These methods quantize an unordered point cloud in a uniform structure like voxels. Some approaches use 3D convolutions to find local relationships between closer groups of points [17, 39]. However, the amount of memory required to compute these convolutions makes them unfeasible to process a large number of points. Methods like OctNet [22] and O-CNN [31] save computation time by using octrees to avoid processing empty spaces. [10] and [23] use Kd-tree and Hash structures instead. [26] uses sparse 3D convolutions rather than efficient data structures. Although these implementations reduce the computation required to train a 3D CNN, quantizing the points comes with the cost of losing important fine-grained information.

Point-based networks. These are networks capable of using irregular point clouds without projecting or quantizing them into regular grids. Their main characteristic is the use of shared MLP layers, also known as point-wise or 1D convolutional layers. PointNet [19] is a milestone of this kind of network. This approach uses MLP layers as permutation-invariant

functions to process each point of a point cloud individually, and a max-pooling layer to aggregate them. The performance of the network is limited because they do not consider local spatial relationships in the data. PointNet++ [20] addresses this issue by sampling the points, grouping them in clusters, and applying PointNet on the clusters. SO-Net [12] uses a similar hierarchical structure adding self-organizing maps (SOMs) to capture better local structures. Other approaches like PointConv [32], PointCNN [13] and KPConv [29] construct kernels based on the input coordinates to be used as convolution weights.

Projection-based approaches. Some works project local neighborhoods into tangent planes and process them with 2D convolutions. The tangent plane parameters can be found using point tangent estimation [27], or approximated [9, 15, 35]. The downside of these approaches is that they lose the information of 1 dimension given that they project the points to a local 2D plane.

Self-attention and transformers. Self-attention and transformers have revolutionized the area of NLP [24, 30]. This has led the 3D segmentation field to investigate these techniques [6, 21, 38]. In the point cloud domain, self-attention networks can be seen as an improvement of the MLP networks, where instead of capturing local relationships by using pooling layers or weighting the features of the neighbors using hard-coded scores [16], they learn these relationships through an attention layer which estimates a score function to weight the contribution of each neighbor. The self-attention architecture resembles the encoder part of the transformers. One of the attempts to apply transformers to point clouds is PCT [6]. They replace the MLP layers from PointNet++ with transformer layers and the output feature of each layer is enriched with a discrete Laplacian operator. There are two differences between PCT and ours. The first one is that they aggregate the points inside a neighborhood by applying maxpooling. We use self-attention instead, which allows the information from all the neighbors to be passed, rather than only using the neighbor with the highest feature value. The second difference is that they use global attention and we use local attention. This means that their method attends to all points, while ours attends to a local cluster of points. In terms of computation, their memory requirements are quadratic $[N \times N]$ while ours is $[K \times N]$ where N is the number of points and K the number of neighbors in the local cluster. [21] uses geometric features to add extra information to semantic features, and self-attention and maxpooling are used to do the local aggregation. The same operation is performed at different scales and the results are combined using another self-attention layer.

The goal of 3D point cloud segmentation is to find good local relationships. Most of the methods use pooling operations [19, 21] to extract the important features inside a patch. However, this loses some information about the neighbors because these operations either return the maximum or average value of a group of points. The neighborhood information can be preserved better by using an attention mechanism, which helps the network to learn how much each neighbor contributes to the local patch. Although there are approaches that use self-attention [6, 20, 21], the type of attention they use is *scalar*. The problem with scalar attention is that it uses the same learned score for all the feature channels of a neighbor point. Our network instead uses vector attention [38], which computes a score for each channel individually, bringing more flexibility to the layer. We extend this flexibility by introducing a two-headed self-attention layer, where one head focuses on geometric features and the other on semantic features. Even though there are works [15, 21] that use geometric and latent features, they treat them indistinguishably, losing the individual contribution of each feature. Our method can also be considered as one of the closest implementations to transformers for point cloud segmentation because, unlike previous research, we adapted one of the key properties of transformers, which is the multi-head attention structure.

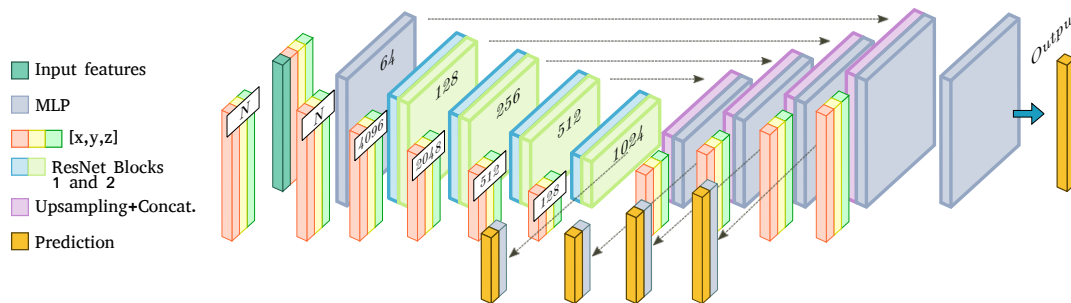


Figure 1: The encoder-decoder architecture receives as input xyz coordinates and RGB . The figure shows the effect of the sub-sample process on the xyz values and the output features of each encoder layer. The encoder consists of ResNet blocks, which have our Ge-Latto layer (see Figure 3). The decoder consists of up-sampling layers which are concatenated with their respective encoder features using residual connections and combined with an MLP.

3 Proposed Method

Ge-Latto extracts two types of information from the point cloud: The geometric information obtained from the Cartesian coordinates of the points and the latent feature information learned by the network each time the point cloud is sub-sampled. The first part of this subsection describes the network architecture and sampling strategy. The second part describes the two-headed attention layer and explains how latent and geometric information is used.

3.1 Network and Sampling

The network has an encoder-decoder architecture and receives as input the xyz coordinates and RGB color. Those features are projected to a higher dimension using a shared MLP layer¹ (see Figure 1). The encoder reduces the number of points and extracts high-level features from a neighborhood of points. For this, each layer sub-samples the number of points of its input. Therefore $N_l > N_{l+1}$ where N is the number of points and l is the layer. The encoder has 4 layers that are designed like bottleneck ResNet blocks [7] with Ge-Latto replacing the 2D convolutions. Using Thomas *et al.* [29] configuration, the input features of a ResNet block are processed by an MLP layer followed by batch normalization and ReLU. The other MLPs of the block are only followed by batch normalization (see Figure 3).

Given the sparse nature of a point cloud, the choice of the sampling method is not trivial. The sampled points have to represent a group of points and be beneficial for the information “aggregation” of its neighbors. Here, we chose Farthest Point Sampling (FPS) because it outputs a more uniform-like distribution which is a desired property for point cloud semantic segmentation [29].

The next step groups each point p_i from the input set \mathcal{P}_l (of size N_l) with their neighbors to find local-spatial relationships. The points can be either grouped by kNN or radius neighbors. We use the latter because it is more robust with non-uniform sampling settings like point clouds [29]. Therefore, for each representative point $p_i \in \mathcal{P}_l$, K points inside the given radius are randomly picked. We use \mathcal{Q}_i to represent the grouped neighboring points of p_i in the rest of the paper. It is important to note that $\mathcal{Q}_i \subseteq \mathcal{P}_{l-1}$, the only exception is in the second ResNet block, where $\mathcal{Q}_i \subseteq \mathcal{P}_l$ because no sampling is carried out; Figure 2 and

¹In the paper, we use the word MLP to refer to a shared MLP layer with 1 hidden dimension.

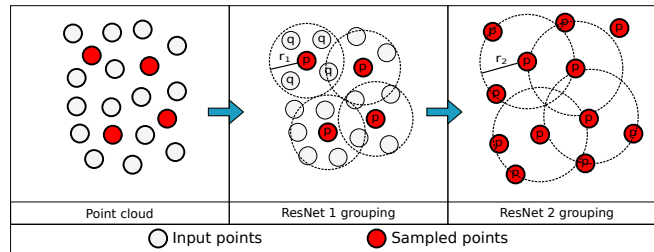


Figure 2: Clustering process inside ResNet blocks. The first image shows the input points of the layer. The grouping criteria of Block 1 and 2 are shown in the second and third image. Block 1 groups the input points using the sampled points as centers with a radius r_1 , whereas Block 2 does the grouping on the sampled points with a bigger radius r_2 .

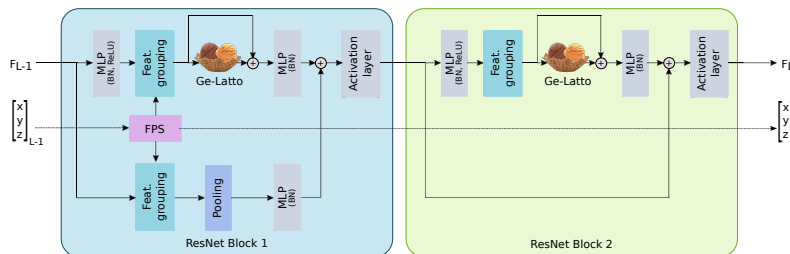


Figure 3: ResNet Blocks. The first block sub-samples the point cloud and finds nearest neighbors inside a radius between the sampled points and the input points. Because of the sampling, the residual connection has a maxpooling layer to match the input with the output size. The function of the second block is similar to the first one, but without sub-sampling.

Figure 3 show an example. The network also increases the receptive field by doubling the radius at every layer.

For segmentation, the decoder up-samples the number of points until it recovers the size of the input of the network. The up-sampling of the features is done via tri-linear interpolation following Lin *et al.* [15]. The interpolated features are concatenated with the features from the corresponding encoder stage thanks to the residual connections (see Figure 1). The final and auxiliary outputs of the decoder are feature vectors for each point in the input point set. An MLP is used to map these features to the final logits, whose feature dimension is the number of classes. The size of the auxiliary outputs corresponds to the number of points their respective layers have. The network has 4 auxiliary outputs, one for the last encoder layer, and three for the following decoder layers. For classification, global average pooling is used over the last encoder features to get a global feature vector of the point cloud. This feature is passed to an MLP to obtain the classification logits.

3.2 Two-headed Attention

We claim that our two-headed attention layer finds better features by combining geometric and latent information in each layer of the encoder (Figure 4). The geometric features that are used are the absolute position of the representative points $p_i \in \mathbb{R}^3$, the K neighbor points $Q_i \in \mathbb{R}^{K \times 3}$, and the relative position of the neighbors $Q_i - \mathcal{K}p_i \in \mathbb{R}^{K \times 3}$, where the operator \mathcal{K} replicates the vector K times. The latent information are the features learned by the hidden layers of the network. Each Ge-Latto layer uses those that belong to each centroid or repre-

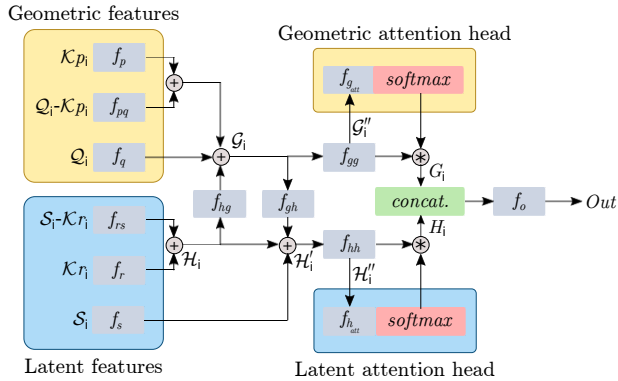


Figure 4: The two-headed Ge-Latto layer computes the local-attention for the geometric and latent features individually and then combines them using f_i MLP layers.

representative point $r_i \in \mathbb{R}^D$, the features of the neighbors $\mathcal{S}_i \in \mathbb{R}^{K \times D}$, and the difference between the K neighbors and centroids features $\mathcal{S}_i - \mathcal{K}r_i \in \mathbb{R}^{K \times D}$, where D is the dimensionality of the features, which is the number of feature planes shown in Figure 1. The feature values are mapped linearly using an MLP layer f_i . The combined geometric and latent features are represented by $\mathcal{G}_i \in \mathbb{R}^{K \times D}$ and $\mathcal{H}_i \in \mathbb{R}^{K \times D}$ respectively, and are computed as follows (see Figure 4): First, the latent features r_i and $\mathcal{S}_i - \mathcal{K}r_i$ are transformed by MLPs and combined by vector addition: $\mathcal{H}_i = f_r(\mathcal{K}r_i) + f_{rs}(\mathcal{S}_i - \mathcal{K}r_i)$.

Then, the geometric features are combined. From Eq. 1, $f_p(\mathcal{K}p_i)$ and $f_q(Q_i)$ encode the global geometric context in 3D space of the representative points and its neighbors. Meanwhile $f_{pq}(Q_i - \mathcal{K}p_i)$ represents the local geometric context. We augment the geometric context by adding and projecting the latent feature \mathcal{H}_i .

$$\mathcal{G}_i = f_p(\mathcal{K}p_i) + f_{pq}(Q_i - \mathcal{K}p_i) + f_q(Q_i) + f_{hg}(\mathcal{H}_i) \quad (1)$$

In the same way, the latent features are combined and augmented by adding the projected geometric feature \mathcal{G}_i . As Eq. 1 encodes the geometric context, Eq. 2 encodes the latent context. $f_r(\mathcal{K}r_i)$ and $f_s(\mathcal{S}_i)$ represent the global latent information and $f_{rs}(\mathcal{S}_i - \mathcal{K}r_i)$ represents the local latent information.

$$\mathcal{H}'_i = \mathcal{H}_i + f_s(\mathcal{S}_i) + f_{gh}(\mathcal{G}_i) = f_r(\mathcal{K}r_i) + f_{rs}(\mathcal{S}_i - \mathcal{K}r_i) + f_s(\mathcal{S}_i) + f_{gh}(\mathcal{G}_i) \quad (2)$$

The resultant features \mathcal{G}_i and \mathcal{H}'_i are each projected by another MLP layer: $\mathcal{G}''_i = f_{gg}(\mathcal{G}_i)$ and $\mathcal{H}''_i = f_{hh}(\mathcal{H}'_i)$. Then, self-attention is used to combine the features inside the neighborhood patch (Eq. 3 and Eq. 4). The attention part consists of an MLP layer followed by a normalization function (Softmax) ϕ to obtain the weights of the neighbor features. Here, vector attention is used instead of scalar attention. This allows the network to “attend” to individual feature channels [38]. The dimension of the attention weights, the geometric features \mathcal{G}''_i and latent features \mathcal{H}''_i is $[K \times D]$. Finally, to aggregate the local features, each neighbor feature $g_k \in \mathcal{G}''_i$ and $h_k \in \mathcal{H}''_i$ is multiplied element-wise by its respective weight and then all the neighbors k are summed; the outputs G_i and H_i have dimension D . In the supplementary material we show how our local aggregation is similar to a Graph NN [2].

$$G_i = \sum_{k=1}^K (\phi(f_{g_{att}}(g_k)) \odot g_k) \quad (3)$$

$$H_i = \sum_{k=1}^K (\phi(f_{h_{att}}(h_k)) \odot h_k) \quad (4)$$

The output O_i of the layer is obtained by concatenating and projecting the geometric and latent features: $O_i = f_o([G_i; H_i])$, where $[G_i; H_i] \in \mathbb{R}^{2D}$ and $f_o : \mathbb{R}^{2D} \mapsto \mathbb{R}^D$.

In the transformers literature [24, 30], the geometric features $f_p(\mathcal{K}p_i)$ and $f_{pq}(\mathcal{Q}_i - \mathcal{K}p_i)$, from Eq. 1, can be seen as absolute and relative positional encodings, respectively. Therefore, Eq. 1 provides information about the absolute position of the points, and the relative position of the neighbor points with respect to the representative (centroid) points. Similarly, $f_{rs}(\mathcal{S}_i - \mathcal{K}r_i)$ from Eq. 2 can be seen as the *key* and *query* components in the transformers settings, where instead of using dot product as similarity function to obtain the relationship between two vectors, the values are subtracted. Each head in our attention mechanism can also be considered as a multi-head attention layer with number of heads $n = D$ or feature dimension $D' = 1$ for each head; see supplementary material for demonstration.

4 Experiments

Our method was evaluated using 3 datasets: ShapeNetPart [33] for 3D object part segmentation, Stanford Large-Scale 3D Indoor Spaces (S3DIS) [1] for 3D scene segmentation, and ModelNet40 [36] for 3D shape classification.

Implementation details: The implementation was built using the public library PyTorch [18]. Adam is used as optimizer with learning rate $1e-4$, $\beta_1 = 0.9$, $\beta_2 = 0.98$, and $\varepsilon = 1e-9$. Cross-entropy with label smoothing is used as loss function for all the outputs. The final loss consists of the sum of 4 auxiliary losses and the main loss: $\mathcal{L} = \alpha_1 * \mathcal{L}_{aux_1} + \alpha_2 * \mathcal{L}_{aux_2} + \alpha_3 * \mathcal{L}_{aux_3} + \alpha_4 * \mathcal{L}_{aux_4} + \mathcal{L}_{main}$. The influence of the auxiliary losses is weighted by α_i because we are only interested in the final prediction, which is optimized by the main loss. Following the results of our ablation study, all the $\alpha_i = 0.4$ in the experiments. The encoder consists of one layer with size N , to process the input features, followed by 4 layers with sizes: 4096, 2048, 512, and 128; as seen in Figure 1. The radius (receptive field) of the first encoder layer with ResNet blocks is $0.10m$ and it doubles at every layer. The number of neighbors is 32 for all the layers except for the last one which is 16. This is because the last layer has fewer points than the rest. All the MLP layers from the ResNet blocks (see Figure 3) are followed by batch normalization and ReLU. The output layer before the prediction consists of an MLP layer with batch normalization and ReLU followed by a dropout with a probability of 0.5. All the experiments were done using a single RTX2080Ti with a batch size of 2. The data augmentation consists of scaling, flipping, rotating, and perturbing the points. For S3DIS, the color was augmented by switching the RGB channels and adding noise.

4.1 Scene Segmentation

The S3DIS [1] dataset was used to test the network for scene segmentation. The dataset consists of six real large-scale indoor areas from three different buildings. Each area has rooms whose points are labeled with 13 classes (e.g. ceiling, floor, chair) and have color information. The number of points in one room varies between 0.5 million to 2.5 million, depending on its size. Because the number of points of each room is large, each room was split into blocks of size $[2m \times 2m \times height]$. For training and testing, 6,144 points were randomly sampled and used as input. However, for testing, 6,144 points are randomly sampled until all the points inside a block are labeled. All the points are only sampled once, except when the total number of points inside a block is not a multiple of 6,144, in that case, the Softmax outputs are summed and the highest value is used as the predicted label. The evaluation metrics used

Method	mIoU	mAcc	ceiling	floor	wall	beam	column	window	door	table	chair	sofa	bookcase	board	clutter
PointNet [19]	41.1	49.0	88.8	97.3	69.8	0.1	3.9	46.3	10.8	59.0	52.6	5.9	40.3	26.4	33.2
SegCloud [28]	48.9	57.4	90.1	96.1	69.9	0.0	18.4	38.4	23.1	70.4	75.9	40.9	58.4	13.0	41.6
FPCConv [15]	62.7	68.9	94.6	98.5	80.9	0.0	19.1	60.1	48.9	80.6	88.0	53.2	68.4	68.2	54.9
MinkowskiNet [3]	65.3	71.7	91.8	98.7	86.2	0.0	34.1	48.9	62.4	81.6	89.8	47.2	74.9	74.4	58.6
KPCConv [29]	67.1	72.8	92.8	97.3	82.4	0.0	23.9	58.0	69.0	81.5	91.0	75.4	75.3	66.7	58.9
PCT [6]	61.3	67.6	92.5	98.4	80.6	0.0	19.4	61.6	48.0	76.6	85.2	46.2	67.7	67.9	52.3
Bilateral [21]	65.4	73.1	92.9	97.9	82.3	0.0	23.1	65.5	64.9	78.5	87.5	61.4	70.7	68.7	57.2
Ge-Latto (ours)	69.2	75.9	94.5	99.2	84.0	0.0	24.5	56.3	68.9	84.2	92.4	82.8	70.9	76.9	64.6

Table 1: S3DIS Area 5 results. The reported metrics are the mean class segmentation (mIoU), mean of class-wise accuracy (mAcc), and IoU for each class.

Method	OA	mIoU	mAcc	ceiling	floor	wall	beam	column	window	door	table	chair	sofa	bookcase	board	clutter
PointNet [19]	78.5	47.6	66.2	88.0	88.7	69.3	42.4	23.1	47.5	51.6	54.1	42.0	9.6	38.2	29.4	35.2
PointCNN [13]	88.1	65.4	88.1	94.8	97.3	75.8	63.3	51.7	58.4	57.2	71.6	69.1	39.1	61.2	52.2	58.6
SPGraph [11]	-	62.1	73.0	89.9	95.1	76.4	62.8	47.1	55.3	68.4	73.5	69.2	63.2	45.9	8.7	52.9
RandLA-Net [8]	88.0	70.0	82.0	93.1	96.1	80.6	62.4	48.0	64.4	69.4	69.4	76.4	60.0	64.2	65.9	60.1
KPCConv [29]	-	70.6	79.1	93.6	92.4	83.1	63.9	54.3	66.1	76.6	64.0	57.8	74.9	69.3	61.3	60.3
Bilateral [21]	88.9	72.2	83.1	93.3	96.8	81.6	61.9	49.5	65.4	73.3	72.0	83.7	67.5	64.3	67.0	62.4
Ge-Latto (ours)	89.7	71.4	81.3	95.3	95.1	82.3	69.2	51.9	64.8	73.3	77.3	59.6	71.1	63.0	67.4	57.9

Table 2: S3DIS dataset k-fold cross-validation comparison table.

are mean class-wise intersection over union (mIoU), mean of class-wise accuracy (mAcc), and overall accuracy (OA). The dataset was evaluated in two ways: 1) Area 5 is used as test set and the network is trained using the other areas. 2) 6-fold cross-validation. Ge-Latto outperforms prior models in both evaluations. On area 5, it is 2.1% better than KPCConv [29] in mIoU (Table 1), the qualitative results are shown in Figure 5. Meanwhile, on the k-fold cross-validation, it obtains the best OA (89.7%), surpassing the previous state of the art of Qiu *et al.* [21] and obtaining better IoU in more objects (Table 2).

4.2 Object Part Segmentation

The performance of our network in object part segmentation is measured by using the ShapeNetPart [33] dataset. This dataset is a collection of 16,681 3D point clouds with 16 categories, each with 2 to 6 part labels. We used the standard train/test splits provided by the dataset. Category mean intersection over union (cat. mIoU) and instance mIoU are used as evaluation metrics. For training, 4096 points are randomly picked and used as input. For testing, the total number of points is used. The evaluation (Table 3) shows that our model is only 0.9% behind the current state of the art in cat. mIoU. Some of the wrong classifications are caused by noisy data, where some object components (e.g. rocket, motorbike, table) are wrongly labeled which is penalized by the metric. Figure 6 shows some qualitative results.

4.3 Shape Classification

The ModelNet40 [36] dataset is used to study the performance of our network for shape classification. The dataset consists of 12,311 3D meshes and their normal vectors classified

Method	ModelNet40	ShapeNetPart	
	OA	cat. mIoU	inst. mIoU
PointNet [19]	89.2	80.4	83.7
PointNet++ [20]	91.9	81.9	85.1
SO-Net [12]	90.9	81.0	84.9
KPCConv [29]	92.7	85.1	86.4
PCT [6]	93.2	-	86.4
Ge-Latto (ours)	91.1	84.2	84.5
Ge-Latto (ours fine-tuned)	93.2	-	-

Table 3: ModelNet40 and ShapeNet comparison table.

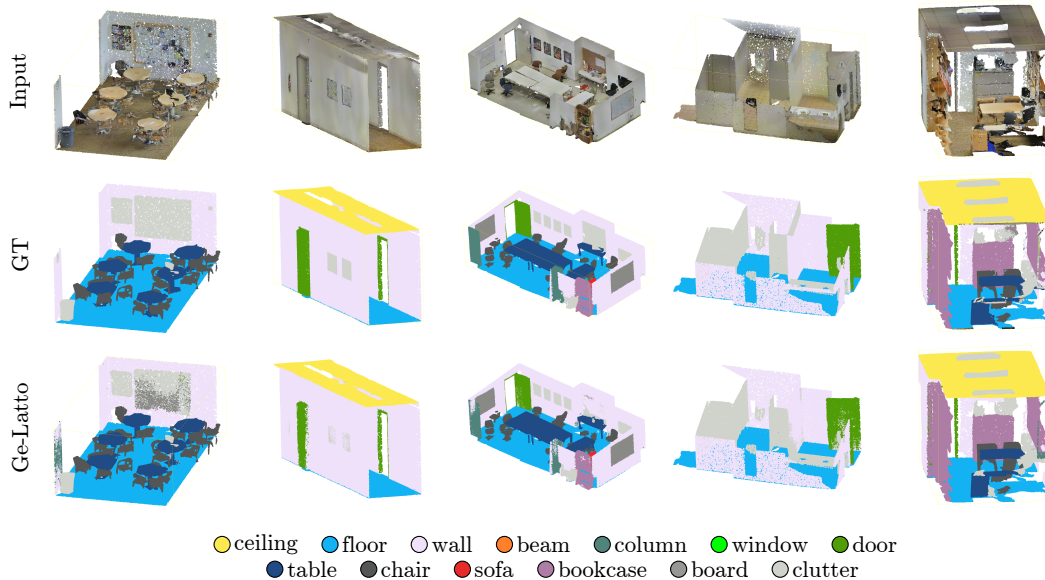


Figure 5: S3DIS results.

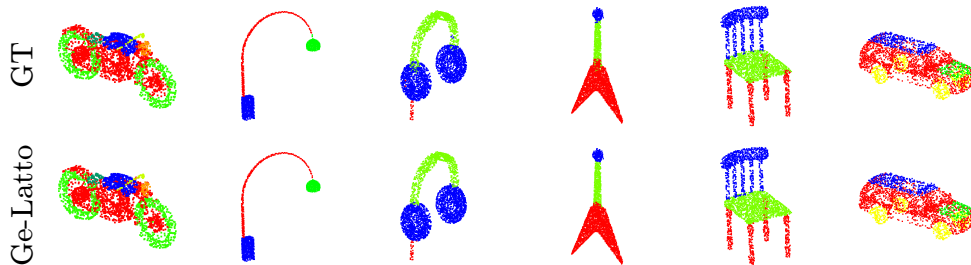


Figure 6: Our ShapeNetPart segmentation results.

into 40 categories. For the experiments, the data is processed similar to Section 4.2. For training, 7,168 points are randomly picked as input, and for testing all the points are used. The evaluation metric is overall accuracy. Our method achieves a competitive result of 91.1% when using the same hyper-parameters and network structure as ShapeNet. If the parameters are fine-tuned, the performance goes up to 93.2%, matching the current best result. More details are given in the ablation study.

4.4 Ablation Study

Auxiliary losses. The auxiliary losses provide a boost in performance to the network. Here, we consider that all weights α_i of the auxiliary losses have the same value and vary them from 0 to 1. Table 4 shows that the best performance is obtained with $\alpha_i = 0.4$, being 1.8% (in terms of mIoU) better than the network trained without auxiliary losses. The supplementary material includes a more comprehensive study for different values of α_i on each loss term.

Two-headed attention. Our proposed attention layer is evaluated using different variants: only with the geometric head, only with the feature head, both heads, and no heads (baseline). For the last one, an MLP+pooling layer replaces the attention mechanism. The experiments reported in Table 4 show that only one head is enough to improve the baseline, and that the combination of both heads helps the network in the segmentation task.

Aux. weight α_i	Auxiliary losses		Attention heads			Number of neighbors			Features per multi-head		
	mIoU	mAcc	Attention heads	mIoU	mAcc	k	mIoU	mAcc	N Feat.	mIoU	mAcc
$\alpha_i = 0.0$	67.4	73.2	Only geometric	66.3	72.0	8	64.5	71.8	1	69.2	75.9
$\alpha_i = 0.2$	68.5	74.4	Only features	66.5	72.3	16	66.4	72.1	2	68.2	74.3
$\alpha_i = 0.4$	69.2	75.9	Both	69.2	75.9	32	69.2	75.9	4	68.0	74.2
$\alpha_i = 0.6$	68.6	74.6	MLP+pooling	63.5	69.2	64	-	-	8	68.0	74.1
$\alpha_i = 0.8$	68.3	74.3									
$\alpha_i = 1.0$	68.1	74.0									

Table 4: S3DIS ablation study experiments.

Number of neighbors. Three networks with different neighborhood size were trained to find the number of neighbors that provide enough local information. The results from Table 4 show that when $k \leq 16$, the number of neighbors might not be enough to provide a correct representation of the local context; $k = 64$ could not fit in the GPU memory.

Features per multi-head. As shown in the supplementary material, each head (geometric and latent) of our attention layer is a special case of a multi-head attention with number of heads $n = D$ or feature dimension $D' = 1$ per head. For this experiment, the number of features D' per head was varied. More features per head means less heads (number of heads $n = D/D'$). In other words, D' features will be weighted by the same attention score. The results from Table 4 demonstrate that the more features a head has (less number of heads), the less flexible the network becomes. However, reducing the number of heads allows the network to be lighter, because it has to compute only D/D' attention scores.

Point cloud classification. The model presented in Section 4 had the same network parameters for all the datasets to show that the proposed method can obtain competitive results without optimizing the hyper-parameters on each dataset. If the hyper-parameters are adjusted for a specific dataset, the performance of the network improves. In this section, the number of sub-sampling points per layer were modified following [34], where they mainly focus on point cloud classification. By sampling the points using the following values per layer, $N \rightarrow 1024 \rightarrow 512 \rightarrow 256 \rightarrow 64$, instead of $N \rightarrow 4096 \rightarrow 2048 \rightarrow 512 \rightarrow 128$, the overall accuracy of our network increases from 91.1% to 93.2%, matching the state-of-the-art result. This seems to be caused by the number of sampled points and the global average pooling at the end of the encoder layer. Considering that the ModelNet40 dataset has objects with similar parts, like plants with flower pots, if one region of the object is bigger than others, this region will have more sampled points. Because the features of the sampled points at the last layer of the encoder are averaged, if there are more points representing a specific area, the averaged features will have a tendency to represent the wrong part of the object.

Work flow video. The video of our proposed method can be found at: <https://youtu.be/mjsttn3C89g>. It shows how the point cloud is sampled during the encoder-decoder phase, the auxiliary outputs, and the learned geometric and latent attention weights.

5 Conclusion

This paper proposes a novel two-headed attention mechanism capable of combining the geometric and latent information of neighbor points to learn richer features. This, combined with the leverage provided by the auxiliary losses, allow our network to work with real data and obtain the state of the art in the complex dataset S3DIS for 3D point cloud semantic segmentation. It also gets competitive results in the ShapeNetPart and ModelNet40 datasets.

References

- [1] Iro Armeni, Ozan Sener, Amir R Zamir, Helen Jiang, Ioannis Brilakis, Martin Fischer, and Silvio Savarese. 3d semantic parsing of large-scale indoor spaces. In *Proceedings of the IEEE Conference on Computer Vision and Pattern Recognition*, pages 1534–1543, 2016.
- [2] Peter W Battaglia, Jessica B Hamrick, Victor Bapst, Alvaro Sanchez-Gonzalez, Viniçius Zambaldi, Mateusz Malinowski, Andrea Tacchetti, David Raposo, Adam Santoro, Ryan Faulkner, et al. Relational inductive biases, deep learning, and graph networks. *arXiv preprint arXiv:1806.01261*, 2018.
- [3] Christopher Choy, JunYoung Gwak, and Silvio Savarese. 4d spatio-temporal convnets: Minkowski convolutional neural networks. In *Proceedings of the IEEE/CVF Conference on Computer Vision and Pattern Recognition*, pages 3075–3084, 2019.
- [4] Hanz Cuevas-Velasquez, Nanbo Li, Radim Tylecek, Marcelo Saval-Calvo, and Robert B Fisher. Hybrid multi-camera visual servoing to moving target. In *2018 IEEE/RSJ International Conference on Intelligent Robots and Systems (IROS)*, pages 1132–1137. IEEE, 2018.
- [5] Hanz Cuevas-Velasquez, Antonio-Javier Gallego, Radim Tylecek, Jochen Hemming, Bart Van Tuijl, Angelo Mencarelli, and Robert B Fisher. Real-time stereo visual servoing for rose pruning with robotic arm. In *2020 IEEE International Conference on Robotics and Automation (ICRA)*, pages 7050–7056. IEEE, 2020.
- [6] Meng-Hao Guo, Jun-Xiong Cai, Zheng-Ning Liu, Tai-Jiang Mu, Ralph R Martin, and Shi-Min Hu. Pct: Point cloud transformer. *arXiv preprint arXiv:2012.09688*, 2020.
- [7] Kaiming He, Xiangyu Zhang, Shaoqing Ren, and Jian Sun. Deep residual learning for image recognition. In *Proceedings of the IEEE conference on computer vision and pattern recognition*, pages 770–778, 2016.
- [8] Qingyong Hu, Bo Yang, Linhai Xie, Stefano Rosa, Yulan Guo, Zhihua Wang, Niki Trigoni, and Andrew Markham. Randla-net: Efficient semantic segmentation of large-scale point clouds. In *Proceedings of the IEEE/CVF Conference on Computer Vision and Pattern Recognition*, pages 11108–11117, 2020.
- [9] Jingwei Huang, Haotian Zhang, Li Yi, Thomas Funkhouser, Matthias Nießner, and Leonidas J Guibas. Texturenet: Consistent local parametrizations for learning from high-resolution signals on meshes. In *Proceedings of the IEEE/CVF Conference on Computer Vision and Pattern Recognition*, pages 4440–4449, 2019.
- [10] Roman Klokov and Victor Lempitsky. Escape from cells: Deep kd-networks for the recognition of 3d point cloud models. In *Proceedings of the IEEE International Conference on Computer Vision*, pages 863–872, 2017.
- [11] Loic Landrieu and Martin Simonovsky. Large-scale point cloud semantic segmentation with superpoint graphs. In *Proceedings of the IEEE conference on computer vision and pattern recognition*, pages 4558–4567, 2018.

- [12] Jiaxin Li, Ben M Chen, and Gim Hee Lee. So-net: Self-organizing network for point cloud analysis. In *Proceedings of the IEEE conference on computer vision and pattern recognition*, pages 9397–9406, 2018.
- [13] Yangyan Li, Rui Bu, Mingchao Sun, Wei Wu, Xinhan Di, and Baoquan Chen. Pointcnn: Convolution on x-transformed points. *Advances in neural information processing systems*, 31:820–830, 2018.
- [14] Tsung-Yi Lin, Priya Goyal, Ross Girshick, Kaiming He, and Piotr Dollár. Focal loss for dense object detection. In *Proceedings of the IEEE international conference on computer vision*, pages 2980–2988, 2017.
- [15] Yiqun Lin, Zizheng Yan, Haibin Huang, Dong Du, Ligang Liu, Shuguang Cui, and Xiaoguang Han. Fpconv: Learning local flattening for point convolution. In *Proceedings of the IEEE/CVF Conference on Computer Vision and Pattern Recognition*, pages 4293–4302, 2020.
- [16] Ze Liu, Han Hu, Yue Cao, Zheng Zhang, and Xin Tong. A closer look at local aggregation operators in point cloud analysis. In *European Conference on Computer Vision*, pages 326–342. Springer, 2020.
- [17] Hsien-Yu Meng, Lin Gao, Yu-Kun Lai, and Dinesh Manocha. Vv-net: Voxel vae net with group convolutions for point cloud segmentation. In *Proceedings of the IEEE/CVF International Conference on Computer Vision*, pages 8500–8508, 2019.
- [18] Adam Paszke, Sam Gross, Francisco Massa, Adam Lerer, James Bradbury, Gregory Chanan, Trevor Killeen, Zeming Lin, Natalia Gimelshein, Luca Antiga, Alban Desmaison, Andreas Kopf, Edward Yang, Zachary DeVito, Martin Raison, Alykhan Tejani, Sasank Chilamkurthy, Benoit Steiner, Lu Fang, Junjie Bai, and Soumith Chintala. Pytorch: An imperative style, high-performance deep learning library. In H. Wallach, H. Larochelle, A. Beygelzimer, F. d'Alché-Buc, E. Fox, and R. Garnett, editors, *Advances in Neural Information Processing Systems 32*, pages 8024–8035. Curran Associates, Inc., 2019.
- [19] Charles R Qi, Hao Su, Kaichun Mo, and Leonidas J Guibas. Pointnet: Deep learning on point sets for 3d classification and segmentation. In *Proceedings of the IEEE conference on computer vision and pattern recognition*, pages 652–660, 2017.
- [20] Charles R Qi, Li Yi, Hao Su, and Leonidas J Guibas. Pointnet++: Deep hierarchical feature learning on point sets in a metric space. *arXiv preprint arXiv:1706.02413*, 2017.
- [21] Shi Qiu, Saeed Anwar, and Nick Barnes. Semantic segmentation for real point cloud scenes via bilateral augmentation and adaptive fusion. *arXiv preprint arXiv:2103.07074*, 2021.
- [22] Gernot Riegler, Ali Osman Ulusoy, and Andreas Geiger. Octnet: Learning deep 3d representations at high resolutions. In *Proceedings of the IEEE conference on computer vision and pattern recognition*, pages 3577–3586, 2017.
- [23] Tianjia Shao, Yin Yang, Yanlin Weng, Qiming Hou, and Kun Zhou. H-cnn: spatial hashing based cnn for 3d shape analysis. *IEEE transactions on visualization and computer graphics*, 26(7):2403–2416, 2018.

- [24] Peter Shaw, Jakob Uszkoreit, and Ashish Vaswani. Self-attention with relative position representations. *arXiv preprint arXiv:1803.02155*, 2018.
- [25] Nicola Strisciuglio, Radim Tylecek, Michael Blaich, Nicolai Petkov, Peter Biber, Jochen Hemming, Eldert van Henten, Torsten Sattler, Marc Pollefeys, Theo Gevers, et al. Trimbot2020: an outdoor robot for automatic gardening. In *ISR 2018; 50th International Symposium on Robotics*, pages 1–6. VDE, 2018.
- [26] Haotian Tang, Zhijian Liu, Shengyu Zhao, Yujun Lin, Ji Lin, Hanrui Wang, and Song Han. Searching efficient 3d architectures with sparse point-voxel convolution. In *European Conference on Computer Vision*, pages 685–702. Springer, 2020.
- [27] Maxim Tatarchenko, Jaesik Park, Vladlen Koltun, and Qian-Yi Zhou. Tangent convolutions for dense prediction in 3d. In *Proceedings of the IEEE Conference on Computer Vision and Pattern Recognition*, pages 3887–3896, 2018.
- [28] Lyne Tchapmi, Christopher Choy, Iro Armeni, JunYoung Gwak, and Silvio Savarese. Segcloud: Semantic segmentation of 3d point clouds. In *2017 international conference on 3D vision (3DV)*, pages 537–547. IEEE, 2017.
- [29] Hugues Thomas, Charles R Qi, Jean-Emmanuel Deschaud, Beatriz Marcotegui, François Goulette, and Leonidas J Guibas. Kpconv: Flexible and deformable convolution for point clouds. In *Proceedings of the IEEE/CVF International Conference on Computer Vision*, pages 6411–6420, 2019.
- [30] Ashish Vaswani, Noam Shazeer, Niki Parmar, Jakob Uszkoreit, Llion Jones, Aidan N Gomez, Lukasz Kaiser, and Illia Polosukhin. Attention is all you need. *arXiv preprint arXiv:1706.03762*, 2017.
- [31] Peng-Shuai Wang, Yang Liu, Yu-Xiao Guo, Chun-Yu Sun, and Xin Tong. O-cnn: Octree-based convolutional neural networks for 3d shape analysis. *ACM Transactions on Graphics (TOG)*, 36(4):1–11, 2017.
- [32] Wenxuan Wu, Zhongang Qi, and Li Fuxin. Pointconv: Deep convolutional networks on 3d point clouds. In *Proceedings of the IEEE/CVF Conference on Computer Vision and Pattern Recognition*, pages 9621–9630, 2019.
- [33] Zhirong Wu, Shuran Song, Aditya Khosla, Fisher Yu, Linguang Zhang, Xiaoou Tang, and Jianxiong Xiao. 3d shapenets: A deep representation for volumetric shapes. In *Proceedings of the IEEE conference on computer vision and pattern recognition*, pages 1912–1920, 2015.
- [34] Tiange Xiang, Chaoyi Zhang, Yang Song, Jianhui Yu, and Weidong Cai. Walk in the cloud: Learning curves for point clouds shape analysis. *arXiv preprint arXiv:2105.01288*, 2021.
- [35] Yuqi Yang, Shilin Liu, Hao Pan, Yang Liu, and Xin Tong. Pfcnn: convolutional neural networks on 3d surfaces using parallel frames. In *Proceedings of the IEEE/CVF Conference on Computer Vision and Pattern Recognition*, pages 13578–13587, 2020.

- [36] Li Yi, Vladimir G Kim, Duygu Ceylan, I-Chao Shen, Mengyan Yan, Hao Su, Cewu Lu, Qixing Huang, Alla Sheffer, and Leonidas Guibas. A scalable active framework for region annotation in 3d shape collections. *ACM Transactions on Graphics (ToG)*, 35(6):1–12, 2016.
- [37] Hengshuang Zhao, Jianping Shi, Xiaojuan Qi, Xiaogang Wang, and Jiaya Jia. Pyramid scene parsing network. In *Proceedings of the IEEE conference on computer vision and pattern recognition*, pages 2881–2890, 2017.
- [38] Hengshuang Zhao, Jiaya Jia, and Vladlen Koltun. Exploring self-attention for image recognition. In *Proceedings of the IEEE/CVF Conference on Computer Vision and Pattern Recognition*, pages 10076–10085, 2020.
- [39] Yin Zhou and Oncel Tuzel. Voxelnet: End-to-end learning for point cloud based 3d object detection. In *Proceedings of the IEEE Conference on Computer Vision and Pattern Recognition*, pages 4490–4499, 2018.

Supplementary Material

Hanz Cuevas-Velasquez¹

hanz.c.v@ed.ac.uk

Antonio Javier Gallego²

agallego@dlsi.ua.es

Robert B. Fisher¹

rbf@inf.ed.ac.uk

¹ School of Informatics
University of Edinburgh
Edinburgh, UK

² Department of Software and Computing
Systems
University of Alicante,
Alicante, Spain

Abstract

This supplementary material is organized as follows: Section **A** demonstrates that our geometric and latent heads are a special case of a multi-head attention layer in the transformers literature. Section **B** shows an example of the prediction of each auxiliary output of the network. Section **C** describes the local aggregation step of our two-headed layer and how it relates to graph neural networks. In Section **D** the geometric and latent attention scores of our Ge-Latto layer are shown. Finally, Section **E** extends the ablation study presented in the main paper.

A Special Case of Multi-head Attention Transformer

Each head (geometric or latent) in our attention mechanism can be considered as a multi-head attention layer with feature dimension (channels) $D' = 1$ for each head or number of heads $n = D$, being D the dimensionality of the features in each layer. This is demonstrated as follows. Considering Eq. 1, the multi-head equation of a feature vector $H_i \in \mathbb{R}^D$ proposed by Vaswani *et al.* [?], where Q_k , R_k and V_k are the query, key and value vectors with size D' .

$$H_i = \text{Concat}(\text{head}_{i,1}, \text{head}_{i,2}, \text{head}_{i,3}, \dots, \text{head}_{i,n})$$

$$\text{head}_{i,n} = \sum_{k=1}^K ((\mathcal{M}\phi(\gamma(Q_k, R_k))) \odot V_k)$$

where :

\mathcal{M} = Replicates the vector D' times

ϕ = Normalization function (1)

γ = Similarity function

$$\dim(\gamma(\cdot)) = 1$$

$$\dim(\text{head}_{i,n}) = D'$$

$$\dim(H_i) = D = nD'$$

K = Neighborhood size

Eq. 1 shows there is one weight ϕ per head n , and each ϕ multiplies D' feature channels. Therefore, **the feature $H_i \in \mathbb{R}^D$ has n weights ϕ and nD' feature channels**. In the case where the number of heads n is D , D' would have the value of 1. There would be one weight ϕ per head, and each weight would multiply one feature channel. **This would give a vector H_i with D weights ϕ and D feature channels**, which are the dimensions of our geometric and latent head features, as seen in Eq. 2 (latent feature equation), or Eq. 3 and Eq. 4 in the main paper.

$$H_i = \sum_{k=1}^K (\phi(f_{h_{att}}(h_k)) \odot h_k) \quad (2)$$

Where the dimension of $f_{h_{att}}(h_k)$, h_k and H_i is D .

B Auxiliary Loss Outputs

Each auxiliary loss optimizes the segmentation output of a sub-sampled version of the point cloud. Figure S1 shows an example of these outputs.

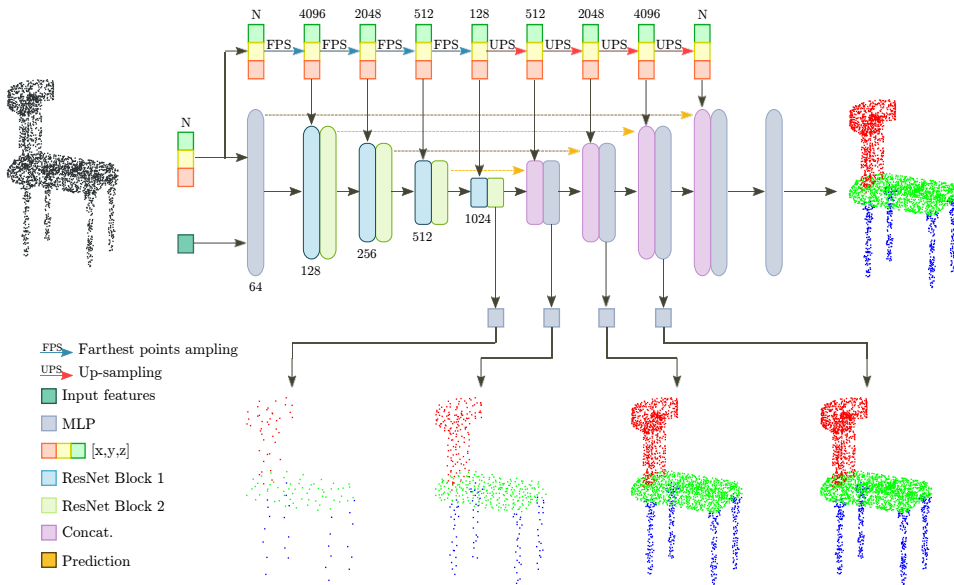


Figure S1: Auxiliary outputs. The network has 4 auxiliary outputs at multiple scales. One output comes from the last encoder layer and the other outputs plus the main output are obtained from the decoder layers.

C Gelatto as a Graph Neural Network

Our network performs local aggregation following steps similar to those that a graph neural network (GNN) uses to update the value of a node through message passing:

- Our network updates the information of each node (center point p_i) based on the information from its neighborhood q_k , preserving graph symmetries (permutation invariance).
- The weights (edges) between the center point and its neighbors are learned through our geometric and latent self-attentions.

- At every step (each new layer of the network), the information from each node is propagated to a further (or neighbor) node until almost all the global information is aggregated.

Table S1 shows this relationship graphically.

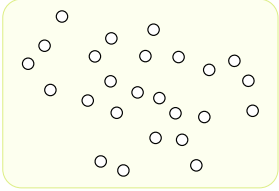
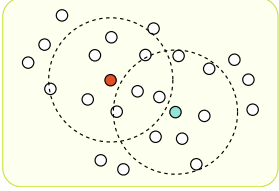
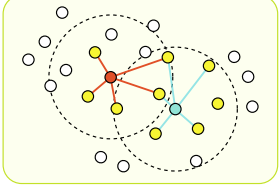
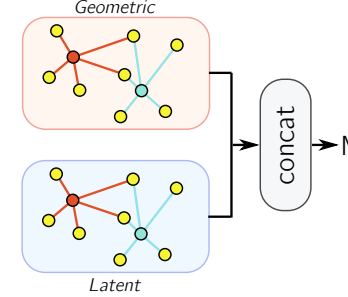
Illustration	Local aggregation (message passing) steps
	<ul style="list-style-type: none"> • Consider a set of points p_i in the point cloud P.
	<ul style="list-style-type: none"> • Our method obtains a local patch around a point by finding all the neighbor points inside a radius r. Here, we visualize the neighborhood of two points, red and cyan.
	<ul style="list-style-type: none"> • The patch is used to create a graph between the center points p_i (red and cyan) and their neighbors q_k (yellow). • To increase the robustness of our network, we randomly chose k neighbors for each centroid. It can be seen as randomly zeroing the value of an edge.
	<ul style="list-style-type: none"> • Our network uses self-attention (Eq. 3 and Eq. 4 in the main paper) to learn the edges that connect a centroid with its neighbors. • The information at a node is updated by aggregating the features from its neighbors and the learned edges. Gelatto creates two graphs, one for the geometric features, and another for the latent features. • After the <i>message passing</i> step, the updated geometric and latent features are concatenated and processed by an MLP layer.

Table S1: Local aggregation process of Gelatto.

D Geometric and Latent Attention Scores

To show the attention scores learned by our Ge-Latto layer after each encoder step, an input point, that was not discarded by the sampling process, was picked. Because the attention score of each point has a dimension D , where D is the dimensionality of a given layer, we randomly picked a value $d \in D$ per attention score to be shown in Figure S2 and Figure S3 for the geometric and latent heads, respectively.

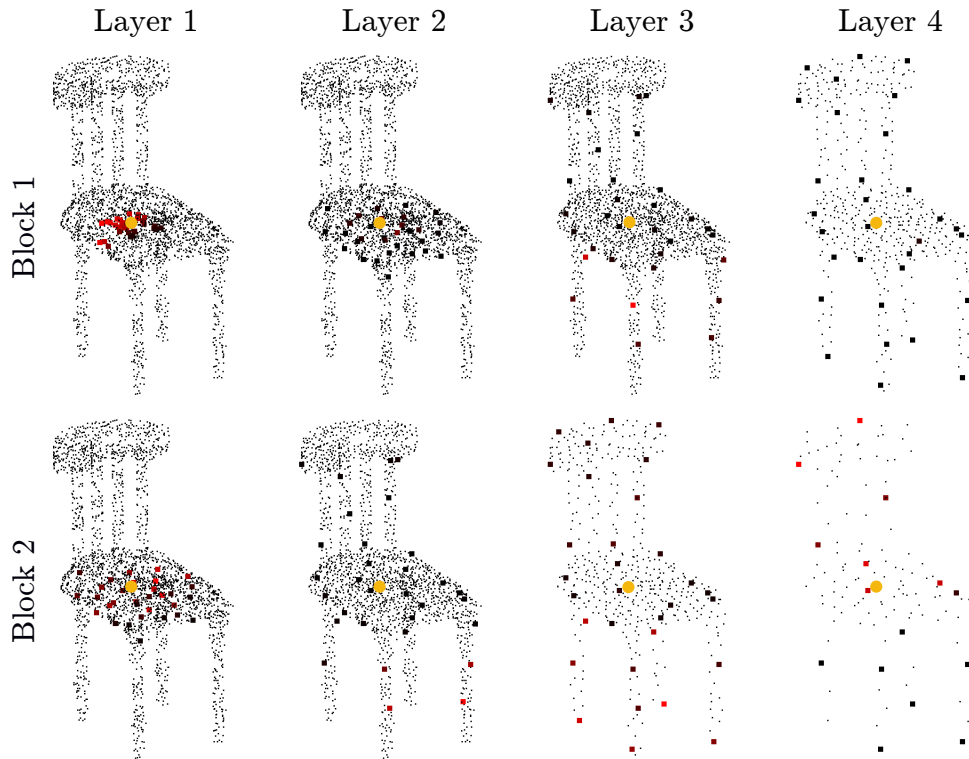


Figure S2: Learned geometric attention scores from a point (in yellow). The attention scores are represented in red, the stronger the intensity, the higher the score. The small black points are the sampled points at a given layer, the bigger points are the selected neighbor points inside a radius. The image shows the attention scores of the two ResNet Blocks at every encoder layer.

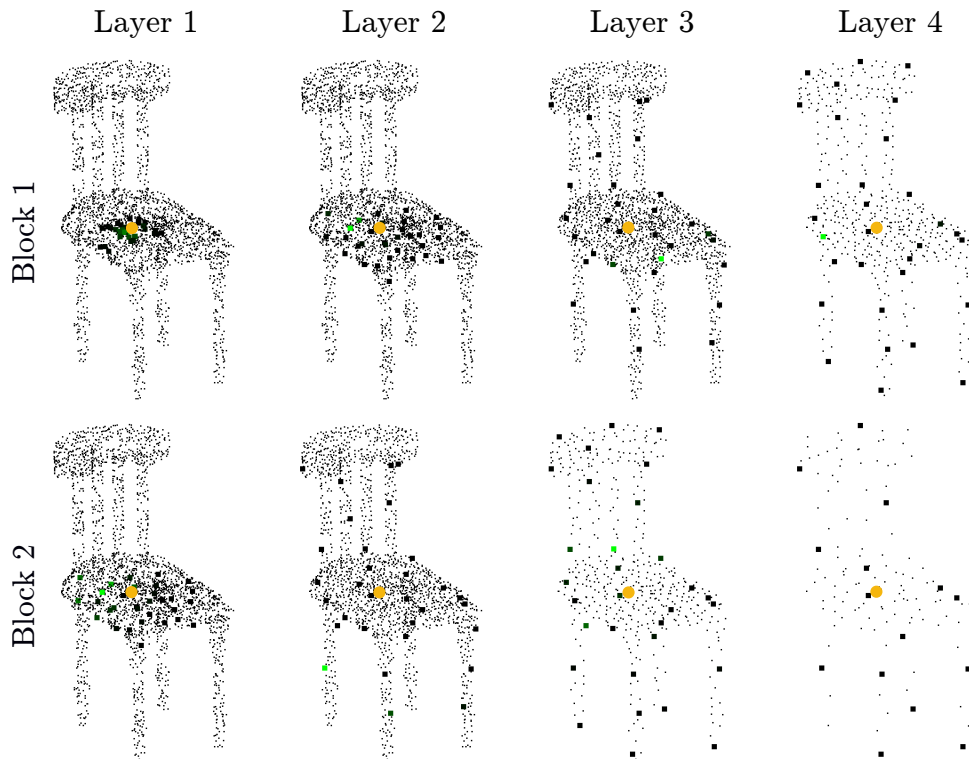


Figure S3: Learned latent attention scores from a point (in yellow). The attention scores are represented in green.

To observe how our network captures global and local relationships, all the attention scores of each head were grouped in Figure S4. The figure shows that, for the chosen point, the latent head focuses more on closer points, meanwhile, the geometric head not only pays attention to the local points but also to more distant points, such as those of the back of the chair and legs.

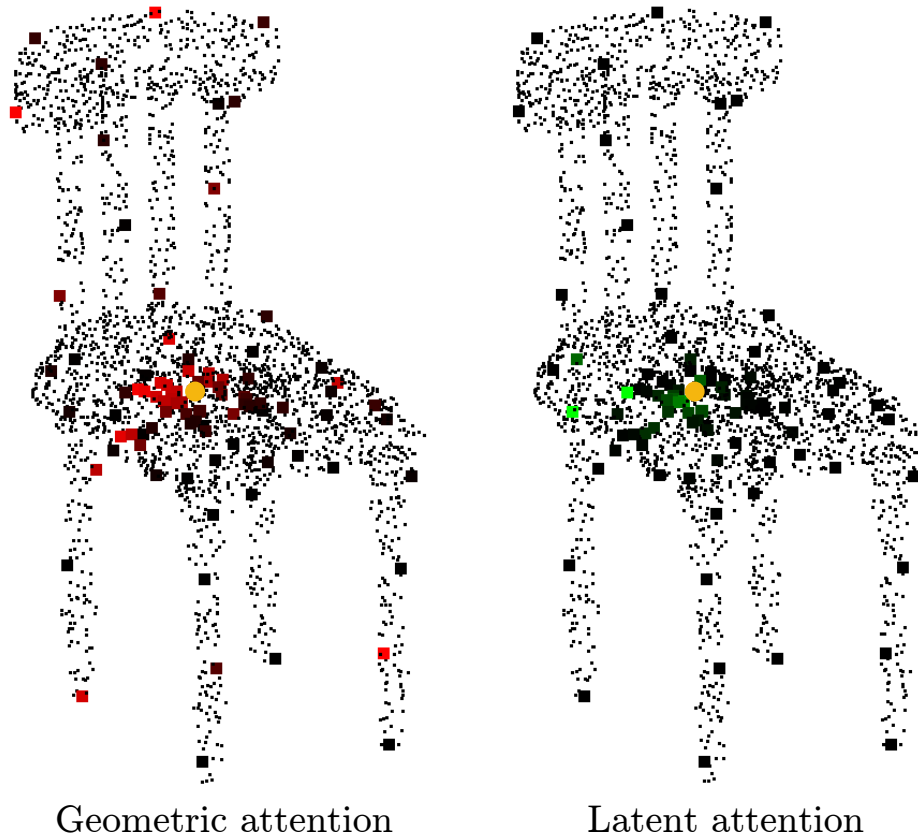


Figure S4: Geometric and Latent attention scores grouped.

E Extended Ablation Study

E.1 Auxiliary losses

In the main paper, we only considered the case when all the auxiliary weights alpha α_i have the same value. This section explores different values for each alpha using grid search. The experiment consists of varying the alpha of one auxiliary loss, from 0 to 1 with increments of 0.2, and fixing the other alphas to 0.4 (the best value found before); the process is repeated for the 4 auxiliary losses. The values that the varying alpha can take are [0, 0.2, 0.6, 0.4, 0.8, 1], where 0 means that we do not minimize the loss for that output. We trained 24 variations of our network (4 auxiliary losses with 6 values for alpha). Each network was initialized with the weights from our best model, for the S3DIS area 5 dataset, and trained for 50 epochs. This experiment showed that there is no improvement when we vary the alphas individually and that the best value for this parameter is 0.4. However, we still observe that the use of auxiliary losses improves the performance of the network. As seen in Table 4 in the main paper, in the ablation study, when the network is trained without auxiliary losses, it obtains an IoU of 67.4%. Meanwhile, when the auxiliary losses are added, the performance increases to 69.2%.

Method	Parameters	mIoU
MinkowskiNet	21.7M	65.3
KPConv	25.8M	67.1
PCT	2.88M	61.3
FPCConv	17.6M	62.7
Ge-Latto (ours)	15.3M	69.2

Table S2: Model parameters comparison table. The parameters are in millions and the metric is for the S3DIS dataset.

Number of points	6K	10K	20K	200K
Inference batch size	5	3	3	3
Inference time	100ms	200ms	210ms	300ms
Training batch size	2	-	-	-
Training time	160ms	-	-	-

Table S3: Training and inference time.

E.2 Model Size and Speed

Table S2 shows that our method achieves the state-of-the-art in the S3DIS dataset with fewer parameters than the previous methods. Our network has only 15.3M parameters, whereas KPConv has 25.8M, MinkowskiNet 21.7M, and FPCConv 17.6M. The only network that has fewer parameters is PCT, 2.88M. However, we are 8% better in point cloud semantic segmentation and obtain a similar performance in ModelNet40.

The training and inference time using different numbers of points and batch sizes are shown in Table S3 reports. This table shows that it takes around 160ms to train 6144 points with a batch size of 2. At inference time, our network can analyze 6144 points with a batch size of 5 in 100ms, 20K points with a batch size of 3 in 210ms, and 200K points with a batch size of 3 in 300ms. All the tests were done using an NVIDIA RTX2080ti. These experiments show that our network is suitable for its applications that need a lighter network.